White matter connections of human ventral temporal cortex are organized by cytoarchitecture, eccentricity, and category-selectivity from birth

Emily Kubota[1*], Xiaoqian Yan[2], Sarah Tung[1], Bella Fascendini[3], Christina Tyagi[1], Sophie Duhameau[1], Danya Ortiz[1], Mareike Grotheer[4,5], Vaidehi S. Natu[1], Boris Keil[5,6,7,8], & Kalanit Grill-Spector[1,9]

1. Department of Psychology, Stanford University, 450 Jane Stanford Way, Stanford, CA 94305, USA
2. Institute of Science and Technology for Brain-Inspired Intelligence, Fudan University, Shanghai, China
3. Department of Psychology, Princeton University, Peretsmfan Scully Hall, Princeton, NJ 08540, USA
4. Department of Psychology, Philipps-Universität Marburg, Frankfurter Str. 35, Marburg 35037, Germany
5. Center for Mind, Brain and Behavior – CMBB, Universities of Marburg, Giessen, and Darmstadt, Marburg 35039, Germany
6. Institute of Medical Physics and Radiation Protection, TH Mittelhessen University of Applied Sciences, Giessen 35390, Germany
7. Department of Diagnostic and Interventional Radiology, University Hospital Marburg, Philipps-Universität Marburg, Baldinger Str., Marburg 35043, Germany.
8. LOEWE Research Cluster for Advanced Medical Physics in Imaging and Therapy (ADMIT), TH Mittelhessen University of Applied Sciences, Giessen 35390, Germany.
9. Wu Tsai Neurosciences Institute, 288 Campus Drive, Stanford, CA 94305 USA

Corresponding author*: emily.kubota@gmail.com

Abstract

Category-selective regions in ventral temporal cortex (VTC) have a consistent anatomical organization, which is hypothesized to be scaffolded by white matter connections. However, it is unknown how white matter connections are organized from birth. Here, we scanned newborn to 6-month-old infants and adults and used a data-driven approach to determine the organization of the white matter connections of VTC. We find that white matter connections are organized by cytoarchitecture, eccentricity, and category from birth. Connectivity profiles of functional regions in the same cytoarchitectonic area are similar from birth and develop in parallel, with decreases in endpoint connectivity to lateral occipital, and parietal, and somatosensory cortex, and increases to lateral prefrontal cortex. Additionally, connections between VTC and early visual cortex are organized topographically by eccentricity bands and predict eccentricity biases in VTC. These data have important implications for theories of cortical functional development and open new possibilities for understanding typical and atypical white matter development.

Introduction

Human ventral temporal cortex (VTC) contains regions that are selective for categories that are important for our everyday lives such as faces[1], bodies[2], words[3], and places[4]. These regions are located in consistent anatomical locations across individuals[5–10]. A key debate in cognitive neuroscience is what structural and functional factors contribute to the consistent functional organization of VTC. One central theory is that innate anatomical constraints and, particularly, white matter connections between VTC and other parts of the brain may lead to the emergence of category-selective regions in consistent anatomical locations relative to cortical folding[11–16]. Indeed, recent research in adults has revealed that the white matter connections of VTC are highly regular with respect to cortical folds[17–19], cytoarchitecture[20], eccentricity[21], and category-selectivity[11,12,22]. However, it is unknown which of these organizing principles of white matter connections of VTC are already present in infancy and if white matter connections remain stable from infancy to adulthood. Here, we address this gap in knowledge by using anatomical and diffusion MRI in infants and adults to elucidate the organization principles of white matter connections of VTC from birth to adulthood.

We first consider multiple hypotheses of how white matter connections at birth may constrain the development of VTC function. The *category hypothesis* suggests that category-selective regions in VTC have category-specific connections forming specialized networks that enable processing of category-specific information[15,23,24].This theory is supported by studies showing that, in adults, white matter connectivity profiles predict the location of face, place, and word-selective regions in VTC[11,22,25] and in children, white matter connectivity profiles at age five predict where word-selective regions will emerge at age eight[13]. Further, functional connectivity of resting state data in infants show category-specific patterns[26,27], suggesting that category-specific networks may be present from birth. The category hypothesis thus predicts that white matter connections of VTC will be organized by category from birth.

The *cytoarchitecture hypothesis* suggests that white matter connections are linked to cytoarchitectonic areas – areas defined by their distribution of cell density across cortical layers[28–30]. VTC contains four cytoarchitectonic areas: FG1-FG4[31,32], which have different neural hardware that is thought to support different functional computations. Notably, in both children and adults, regions with different category-selectivity within the same cytoarchitectonic area, e.g., face-selective and word-selective regions located in FG4, have similar white matter connectivity profiles[20]. But regions with the same category-selectivity located in different cytoarchitectonic regions, e.g., face-selective regions located in FG2 and FG4, respectively, have different white matter connectivity profiles[20]. The cytoarchitectonic hypothesis therefore predicts that white matter connections of VTC will be organized by cytoarchitecture from birth.

The *eccentricity-bias hypothesis* suggests that eccentricity biases in VTC are due to innate white matter connections with early visual cortex (EVC, union of V1-V2-V3), where faces and word-selective regions have more connections with foveal EVC and place-selective regions have innate

white matter connections with peripheral EVC. This theory is supported by findings that in both children and adults, face and word-selective regions in VTC have a foveal bias[5,7,8,33], whereas place-selective regions in VTC have a peripheral bias[5,7,8,33]. Additionally, patterns of functional connectivity between face- and place-selective regions in VTC and EVC in infant humans, neonate monkeys, and congenitally blind adults follow eccentricity bands[34–38]. That is, face-selective regions have higher functional connectivity to central eccentricity bands in EVC and place-selective regions have higher functional connectivity to peripheral eccentricity bands in EVC. Finally, in adults, white matter connections between VTC and EVC also correspond to eccentricity bands, with face-selective regions having more connections to central EVC eccentricities and place-selective regions having more connections to peripheral ones[21]. Therefore, the eccentricity-bias hypothesis predicts that the subset of white matter connections between VTC to EVC will have a non-uniform distribution, where regions in VTC that have foveal bias in adults (faces and words) will have more connections with central bands in EVC from birth, and regions that have a peripheral bias (places) will have more connections with peripheral bands in EVC from birth.

In addition to the unknown organizational principles of white matter connections in infancy, it is also unknown if white matter connectivity profiles are stable or change over development. Accumulating evidence reveals that the large fascicles (axonal bundles that travel in parallel connecting distant parts of the brain) are present at birth[39–43]. Nonetheless, some fascicles continue to develop after birth. For example, the arcuate fasciculus (AF), which connects the VTC with lateral prefrontal cortex is not fully developed in infancy: it has a smaller cross section in children compared to adults[44] and, and in infants, it reaches premotor cortex but not lateral prefrontal cortex as it does in adults[45]. Additionally, mature white matter connections in adulthood may depend on visual experience as visual deprivation during infancy and childhood leads to degradation of white matter tracts of the visual system[46–50]. However, it is unknown which aspects of VTC white matter connectivity profiles are innate and which aspects may develop from infancy to adulthood.

To address these key gaps in knowledge, we obtained diffusion magnetic resonance imaging (dMRI) and anatomical MRI in infants and adults and evaluated the organization and development of white matter connections of category-selective regions of VTC.

Results

We collected MRI data from 44 newborn to 6-month-old infants (26 longitudinally) during natural sleep using 3T MRI over 77 sessions, as well as from 21 adults (28.21$\pm$5.51 years), obtaining whole brain anatomical MRI (T1-weighted, T2-weighted) and multishell dMRI data in each participant. We implemented several quality assurance measures to ensure high quality data (see Methods: Quality Assurance). Four infant sessions were excluded because of missing diffusion data, and six infant

sessions were excluded after quality assurance. We report data from 67 infant sessions (21 longitudinal infants) and 21 adult sessions with no significant differences in data quality (see Methods). In total, we report data from 88 sessions: 23 sessions from newborns (mean age±standard deviation: 28.6±10.2 days), 23 sessions from 3-month-olds (106.9±19.3 days), 21 sessions from 6-month-olds: (189.0±15.8 days), and 21 sessions from adults (28.21±5.51 years). Anatomical MRIs were used to segment the brain to gray and white matter, define the gray-white matter boundary to seed the tractography, and create cortical surface reconstructions. dMRI data was used to derive the whole brain white matter connectome of each individual and session.

To determine how white matter connections are organized in infants and adults and how they may constrain the development of regions in VTC, we project adult functional regions of interest (fROIs) to the native space of each individual and determine the white matter connections of each fROI. We reason that this procedure enables determining the relationship between white matter connectivity in infancy and the eventual location of each fROI in adulthood. To do so, we use cortex based alignment[51] to project maximal probability maps (MPMs) of adult category-selective regions from independent data[20] into each individual brain and session. MPMs of fROIs selective for faces, bodies, and places (mFus-faces, pFus-faces, OTS-bodies and CoS-places) are bilateral, and MPM fROIs selective for words (mOTS-words and pOTS-words) are in the left hemisphere only (Fig 1A,B). We measure the surface area of fROIs relative to the surface area of each hemisphere in all infant and adult sessions and test if the relative fROI size changes over development (as developmental effects plateau, we use a logarithmic model: fROI size/surface area ~ log10(age in days)). We find no development as the relationship between the surface area of fROIs relative to hemisphere surface area does not change with age ($t(878) = 8.77x10^{-6}$, $p = 0.88$). We also visually inspected in each infant and adult session the location of fROIs and cytoarchitectonic areas relative to the cortical folding to test if there is a consistent relationship across age. We find that both fROIs and cytoarchitectonic areas are aligned to the expected anatomical landmarks in nearly each infant (fROIs; LH: 66/67, RH: 65/67, cytoarchitectonic areas; LH: 67/67, RH: 62/67) and adult (fROIs: LH: 21/21, RH: 21/21, cytoarchitectonic areas; LH: 20/21, RH: 21/21) (Supplementary Figs 1-8). For example, as in prior studies[20,52] CoS-places aligns to the intersection of the anterior lingual sulcus and collateral sulcus[6,9], and the boundaries between F1 and FG2 and between FG3 and FG4 are aligned to the MFS. Therefore, in both infants and adults there is a consistent relationship between category-selective regions and cytoarchitectonic areas[20,52], where MPMs for pOTS-words and pFus-faces are within FG2, CoS-places is within FG3, and mFus-faces, OTS-bodies, and mOTS-words are within FG4 (Fig 1C).

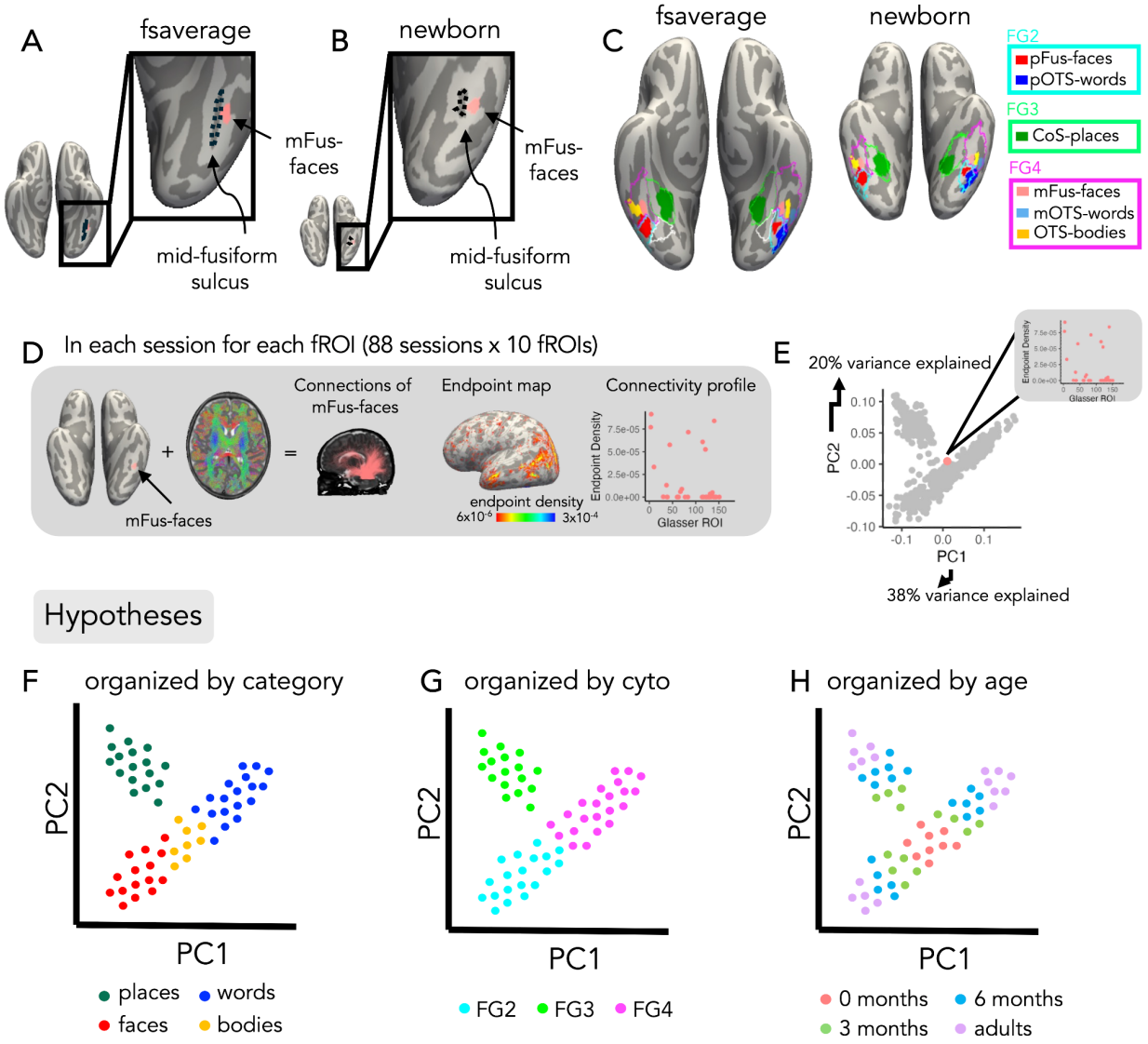

Figure 1. Functional atlas and analysis pipeline. A) mFus-faces aligns to the mid-fusiform sulcus in the fsaverage brain space (left) and B) the newborn brain space (right). C) *Left:* Functional region of interest (fROI) atlas from 28 adults in[20] and Atlas of cytoarchitectonic areas from[53] projected to the fsaverage brain; *Right:* the same atlases projected into an example newborn's brain (17 days old). Solid colors represent fROIs. Salmon *pink:* mFus-faces (mid fusiform face-selective region); *Light blue:* mOTS-words (mid occipital temporal sulcus word-selective region); *Yellow:* OTS-bodies (occipital temporal sulcus body and limb-selective region); *Red:* pFus-faces (posterior fusiform face-selective region); *Blue: p*OTS-words (posterior occipital temporal sulcus word-selective region). Green: CoS-places (collateral sulcus place-selective region). Outlines represent cytoarchitectonic areas[53]. *Cyan:* FG2; *Green:* FG3; *Magenta:* FG4. Both fROIs and cytoarchitectonic areas align to the expected anatomical landmarks in the newborn. All individuals data in Supplementary Figs 1-8. D) Pipeline to define white matter connectivity profiles for each fROI. *Left:* example connections of mFus-faces in an individual newborn participant; *Middle*: endpoint map on the cortical surface; *Right:* quantification of endpoint density within each Glasser ROI. E) Principal Components Analysis (PCA) plot across the first two PCs: PC1 explains 38% percent of the variance, and PC2 explains 20% percent of the variance. Each dot represents a single connectivity profile in a single subject, the salmon pink dot represents the connectivity profile shown in (D). (F-H) Schematic illustrating predictions of three hypotheses in PC space. Each dot represents a connectivity profile for a given fROI and session. (F) Category hypothesis: schematic demonstrating what the data might look like if the connectivity profiles were organized by category. *Green:* place-selective, *blue:* word-selective, *red:* face-selective, *yellow:* body-selective. G) Cytoarchitectonic

hypothesis: schematic demonstrating what the data might look like if the connectivity profiles were organized by cytoarchitecture. *Cyan:* FG2, *green:* FG3, *magenta:* FG4. H) Age hypothesis: schematic demonstrating what the data might look like if the connectivity profiles were organized by age. *Salmon pink:* 0-months, *green:* 3 months, *blue:* 6 months, *purple:* adults.

We use a data-driven approach to determine the organizing principles of white matter connections of VTC. As the category and cytoarchitecture hypotheses make predictions about connectivity across the whole brain, whereas the eccentricity-bias hypothesis makes predictions only about connectivity with EVC, we first test if white matter connections of whole brain connectivity profiles are organized by category-selectivity or cytoarchitecture. In addition, we test if whole brain connectivity profiles are organized by age to determine if connectivity profiles are stable or changing over development. We separately examine the eccentricity-bias hypothesis in the next section.

We derive each fROI's white matter connections by intersecting each fROI with the whole brain white matter connectome derived from dMRI in each session (Fig 1D). We quantify the white matter connectivity profile by measuring the endpoint density of each fROI's connections on the whole brain as the proportion of connections ending in each of 169 Glasser Atlas ROIs[54] (180 Glasser ROIs excluding 11 VTC ROIs, Fig 1D). This results in 880 unique connectivity profiles (10 fROIs x 88 sessions across infants and adults). Then we use principal component analysis (PCA) to reduce the dimensionality of the connectivity profiles. The first 10 principal components (PCs,) explain 98% of the variance in the data, with the first and second components explaining 38% and 20%, respectively.

To visualize how connectivity profiles cluster, we plot the connectivity profiles of all fROIs and sessions in PC space (Fig 1E). The plot consists of 880 dots including data from all infant and adult participants, where each dot represents a single connectivity profile of an fROI from one session. Note that each white matter connectivity profile has several non-mutually exclusive features: the category-selectivity of the fROI, the cytoarchitectonic area in which the fROI is located, and the age of the participant. Therefore, we can label each connectivity profile by each of these features (category, cytoarchitecture, age group) and test if connectivity profiles cluster by one or more of these features. For example, if connectivity profiles are organized by category, then connectivity profiles of fROIs with the same category-selectivity would be nearby in PC space, and separate from connectivity profiles of fROIs with a different category-selectivity (Fig 1F). However, if connectivity profiles are organized by cytoarchitecture, then connectivity profiles of fROIs in the same cytoarchitectonic area would be nearby in PC space (Fig 1G). Further, if connectivity profiles change across development, then connectivity profiles of newborns may be different than other age groups and connectivity profiles of adults may be most distinct (Fig 1H).

Labeling connectivity profiles by fROIs' preferred category reveals some clustering by category (Fig 2A). For example, connectivity profiles of face- and place-selective ROIs tend to be clustered and separate from others. However, clustering by category is imperfect, as connectivity profiles of

word-selective regions split into two clusters, and there is overlap between the connectivity profiles of word- and body-selective fROIs. In contrast, labeling connectivity profiles by fROIs' cytoarchitectonic area reveals a strikingly clear organization whereby connectivity profiles of each of the cytoarchitectonic areas FG2, FG3, FG4 form a different cluster with a distinct connectivity profile (Fig 2B). Examination of the PC loadings (Supplementary Fig 9) and the coefficients across the first 2 PCs suggests that connectivity profiles of fROIs in different cytoarchitectonic areas largely vary in their connections to early visual, lateral occipito-temporal, and anterior temporal cortex. Finally, labeling connectivity profiles by participant's age group reveals that connectivity profiles are intermixed across age groups with no clear organization by age across the first 2 PCs (Fig 2C).

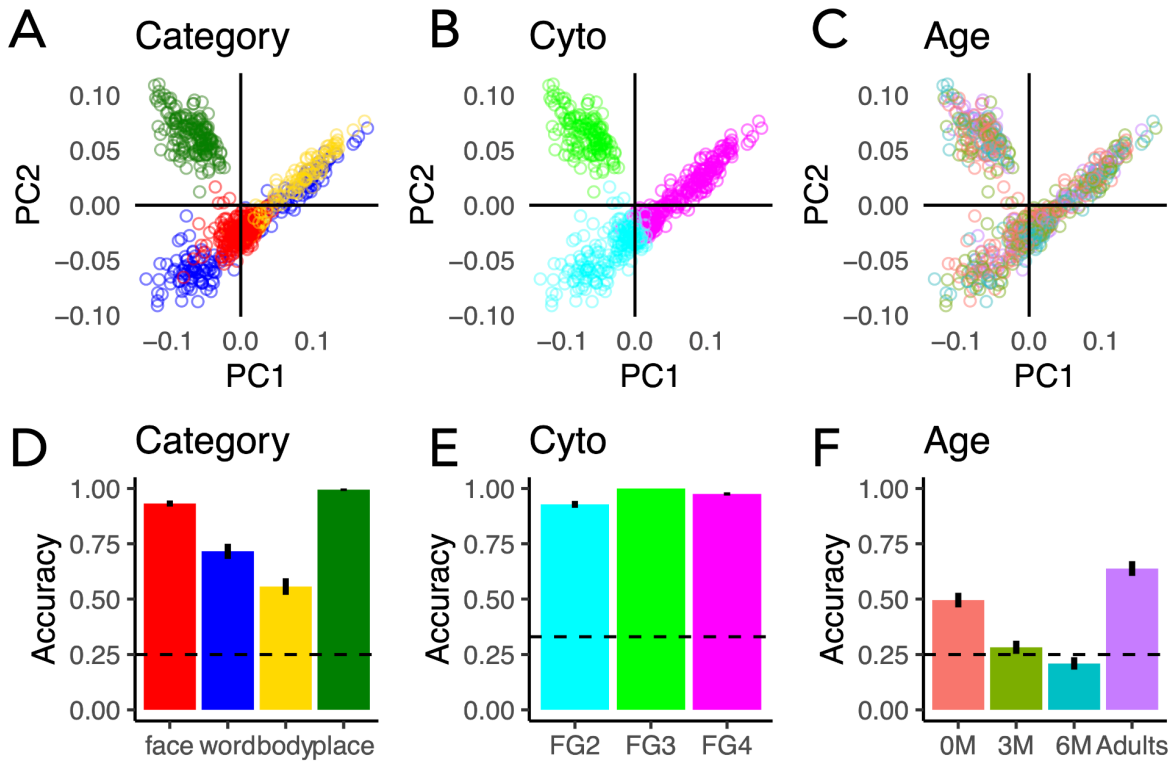

Figure 2. White matter connections are organized by cytoarchitecture and category from infancy. (A-C) White matter connectivity profiles of all participants and fROIs projected to the first two principal components (PC1 and PC2); each dot is a connectivity profile of a single fROI and session. The same data is shown in all three panels, except that they are labeled in color by different features. (A) Category: *red*: faces, *green:* places, *blue*: words, *yellow:* bodies, (B) Cytoarchitectonic area: *cyan:* FG2, *green:* FG3, *magenta:* FG4. (C) Age group: *salmon:* newborn, *green:* 3 months, *teal:* 6 months, *purple*: adults. (D-E) Classification accuracy of a feature from white matter connectivity profiles, using multinomial logistic regression with leave-one-out-participant cross validation. (D) Classification accuracy of category. (E) Classification accuracy of cytoarchitectonic area. (F) Classification accuracy of age group. In D-F, *bar:* mean performance across participants; *Error bars*: standard error of the mean across participants; *Dashed line*: chance level.

To utilize the information across all 10 PCs, we use a leave-one-out classification approach to test if a classifier trained on white matter connectivity profiles of n-1 participants can predict the category preference, cytoarchitectonic area, or the participant's age group from the left out participant's connectivity profiles. We find that category (Fig 2D, mean accuracy±SD = 83%±10%, t(87) = 47.09, $p < 2.2x10^{-16}$), cytoarchitecture (Fig 2E, mean accuracy±SD= 97%±5%, t(87) = 109.6, $p < 2.2x10^{-16}$), and age (Fig 2F, mean accuracy±SD = 41%± 27%, $t(87) = 5.48$, $p < 3.99x10^{-7}$) are all classified significantly above chance. Classification of cytoarchitecture is significantly higher than classification of category preference (odds ratio= 5.96, 95% CI [3.98 8.93], binomial logistic regression) and age (odds ratio = 41.51, 95% CI [28.16, 61.19], binary logistic regression). Confusion matrices reveal almost no error for cytoarchitecture classification (Supplementary Fig 10A), but some category errors that arise from confusion of word-and body-selectivity as well as confusion of body and face-selectivity (Supplementary Fig 10B). The confusion matrix for age classification (Supplementary Fig 10C) reveals that newborns and adults are classified the best, that 3 month-olds are often confused for newborns, and that 6 month-olds are equally confused across all age groups. This suggests that there is heterogeneity in the connectivity profiles of 6-months-olds, and that around 6 months of age, the white matter connections of some infants may start to become more adult-like.

To assess if the high classification performance of cytoarchitecture is due to higher anatomical proximity of fROIs within the same cytoarchitectonic area compared to those in distinct cytoarchitectonic areas, we repeat the classification analysis on connectivity profiles of equidistant disk ROIs that are either in the same (FG4) or different (FG2/FG4) cytoarchitectonic areas (Supplementary Fig11A,B). We reason that if anatomical proximity drives classification results, then classification accuracy will be reduced once distance is controlled. However, even when distance was held constant, cytoarchitecture is classified from the connectivity profiles with high accuracy (Supplementary Fig11C, mean accuracy±SD=95%±22%, t(87) = 31.62, $p < 2.2x10^{-16}$), suggesting that organization of connectivity profiles by cytoarchitecture is not just due to anatomical distance between fROIs.

Interestingly, both category and cytoarchitecture classification are not significantly different across age groups (comparison between newborns, 3-month-olds, and 6-month-olds compared to adults (newborns: odds ratio =1.20, 95% CI [0.77, 1.89], 3-months: odds ratio =1.01, 95% CI [0.65, 1.56], 6-months: odds ratio =1.05, 95% CI [0.67, 1.65], binomial logistic regression). Indeed, examination of the organization structure across the first 2 PCs separately for each age group reveals similar organization across age groups (Supplementary Fig 12). These analyses suggest that organizational features of white matter connections by cytoarchitecture and category persist across development.

253 *Are White Matter Connections Between VTC and Early Visual Cortex Organized Retinotopically?*

254 To test the eccentricity-bias hypothesis we next examined the subset of connections between each
255 fROI and early visual cortex (EVC). We reasoned that if connections between VTC and EVC are
256 organized by eccentricity from birth, then fROIs that overlap with foveal representations in adults
257 (pFus-faces, pOTS-faces, mFus-faces, OTS-bodies, mOTS-words) would have more white matter
258 connections to central than peripheral eccentricities in EVC in infancy, and fROIs that overlap with
259 peripheral representations in adults (CoS-places) would have more connections to peripheral than
260 central eccentricities in VTC in infancy. To test these predictions, we measured the distribution of
261 white matter endpoints between each of the VTC category-selective fROIs and three eccentricity
262 bands in EVC: 0-5°, 5-10°, and 10-20° and compared across age groups.

263 We first visualized the white matter connections between each fROI and EVC, coloring the white
264 matter connections according to the endpoint eccentricity in EVC. This visualization reveals a
265 striking orderly arrangement of the connections from each eccentricity band to each of the fROIs
266 in both infants and adults (Fig 3A and 3B; see Supplementary Videos 1-4 for 3D visualization).
267 Specifically, in all age groups, newborns to adults, there is a lateral to medial arrangement of
268 connections such that connections to EVC central eccentricities (red, 0-5°) are more lateral, and
269 connections to more peripheral EVC eccentricities are more medial (green, 5-10° to blue, 10-20°;
270 Fig 3A,B).

271 We then quantified the distributions of endpoint connections to EVC for each fROI and age group.
272 Consistent with the predictions of the eccentricity-bias hypothesis, in all age groups, pFus-faces,
273 pOTS-words, mFus-faces, OTS-bodies, and mOTS-words had more connections to the EVC 0-5°
274 eccentricity band than the more peripheral eccentricities (Fig 3C) and CoS-places had more
275 connections to the EVC 10-20° eccentricity band than to the more central eccentricities (Fig 3C).
276 Additionally, the connections from VTC to EVC by eccentricity band also mirror the
277 cytoarchitectonic organization of the VTC connectivity profile. Specifically, across all age groups:
278 (i) pFus-faces and pOTS-words, which are located in cytoarchitectonic area FG2, have ~60% of
279 their connections to the EVC 0-5° eccentricity band, whereas (iii) CoS-places, which is located in
280 FG3, has ~40% of its connections to the EVC 10-20° eccentricity band, and (iii) mFus-faces, OTS-
281 bodies, and mOTS-words in FG4 have 40-50% of their EVC connections in the central 5° (Fig 4C).

282 We further tested how eccentricity is related to the features of cytoarchitecture, category, and age
283 that we examined in the whole brain analysis. To do so, for each fROI we fit a linear model predicting
284 the percentage of connections to the central 5° by cytoarchitecture, category-selectivity, and age
285 group. As the percentage of connections to each eccentricity band is proportional, we use the
286 percentage of connections to the central 5° as the independent variable, where a greater
287 percentage connections to the central 5° indicate more connections to central eccentricity bands,
288 and fewer connections to the central 5° indicate more connections to peripheral eccentricity bands.

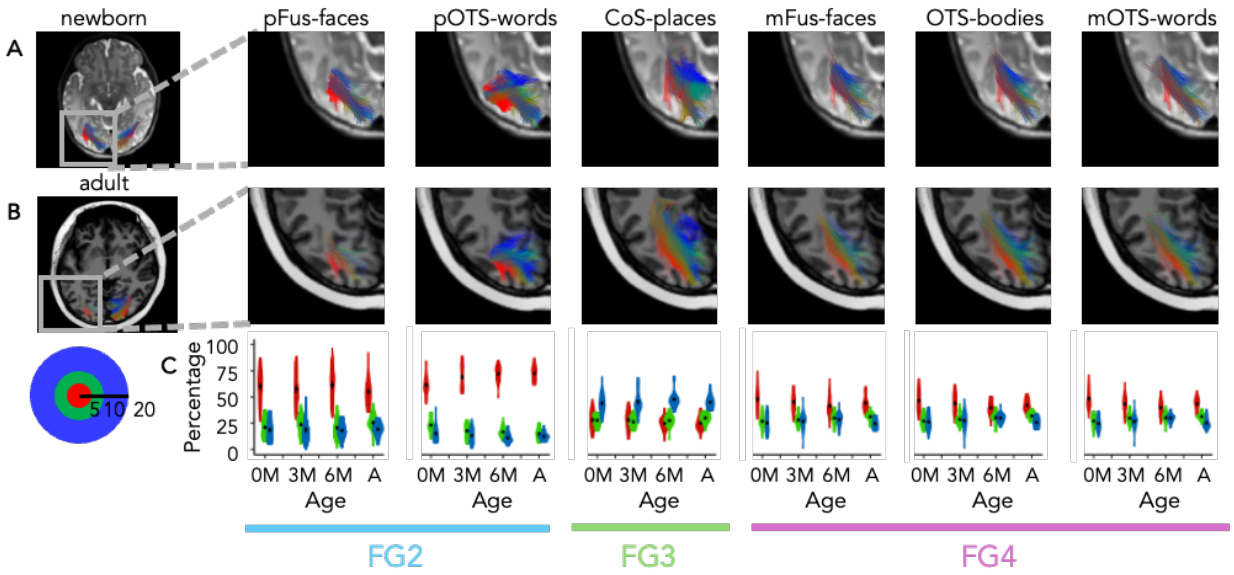

Figure 3. White matter connections of VTC are organized by eccentricity from birth. Connections between each fROI and early visual cortex (EVC, union of V1, V2, V3) in an example newborn (A) and an example adult (B). Here we report data for the left hemisphere as it includes all 6 fROIs; data for the right hemisphere is reported in Supplementary Fig 53. Connections are colored by the endpoint eccentricity band in EVC: *red:* 0-5°, *green*: 5-10°, *blue:* 10-20°. (C) Quantification of the percentage of endpoints in each eccentricity band by age group for each fROI: Violin plots indicate distributions of the percentage of connections for each age group and eccentricity band. Black dot and error bar indicates mean± standard error of the mean. *Red:* 0-5°, *green*: 5-10°, blue: 10-20°, see inset. *0M:* newborns, *3M:* 3 month-olds, *6M:* 6 month-olds, A: adults. Horizontal lines in the bottom indicate cytoarchitectonic area..

We find a main effect of cytoarchitecture ($F(2,504) = 390.02$, $p < 2.2\times10^{-16}$), suggesting that regions that are in distinct cytoarchitectonic areas have different percentages of connections going to the EVC central 5°. In particular, FG2 has a majority of its connections going to the central 5° in EVC, but FG3 has a minority (mean±sd: FG2: 63.57%±14.41%, FG3: 26.58%±8.33%, FG4: 43.97%±9.34%). Additionally, there is a main effect of category-selectivity ($F(2,504) = 8.32$, $p= 0.0003$), reflecting that regions with different category-selectivity also have different percentages of connections going to the EVC central 5°. Face- and word-selective regions have a majority of connections going to the central 5°, but place-selective regions have only a minority (mean±sd: faces: 51.70%±15.02%, words: 56.21%±15.73%, places: 26.58%±8.33%, bodies: 43.23%±9.05%). In contrast, there is no main effect of age group ($F(3,504) = 1.14$, $p = 0.33$), and no significant interaction between category and age ($F(6,504) = 0.93$, $p = 0.47$). There are, however, significant interactions between cytoarchitecture and category ($F(1,504) = 24.55$, $p = 9.91\times10^{-7}$), cytoarchitecture and age ($F(6,504) = 3.59$, $p = 0.002$), and between cytoarchitecture, category, and age ($F(3,504) = 2.76$, $p = 0.04$). Post-hoc tests reveal that the cytoarchitecture by category interaction is driven by differences in percentage of connections to the central 5° between pFus-faces and pOTS-words in FG2 ($t(87) = 5.68$, $p = 1.77 \times 10^{-7}$), as well as differences in percentage of connections to the central 5° between mFus-faces and OTS-bodies in FG4 ($t(87) = 3.68$, $p = .0004$). Further post-hoc tests reveal that differential development is due to a decrease in the percentage of connections from FG4 to the EVC central 5° over development ($\beta = -2.75$, $t(163.09) = -3.39$, $p = 0.0009$), and a differential development within FG2 where there is a significant increase in the

connections of pOTS-words to the central 5° over development (β = 3.95, t(81.26) = 3.52, p = 0.0007), but no significant development in the percentage of pFus-faces connections to the central 5° (β = -0.78, *t*(85.90) = -0.47, *p* = 0.64). These results suggest that in addition to cytoarchitecture, and category, white matter connections of VTC are organized topographically by eccentricity from birth and that the differential proportion of connections between VTC to different eccentricity bands from birth mirrors the eccentricity bias of both cytoarchitectonic areas and category-selective regions in VTC.

Do White Matter Connectivity Profiles of VTC Develop from Infancy to Adulthood?

In addition to revealing the organizing principles of white matter connections by cytoarchitecture, category, and eccentricity, we also found evidence for development as we were able to classify the age group of the participant above chance from the whole connectivity profile, and we find some developmental changes in connectivity with EVC. To qualitatively assess how the whole brain white matter connections of VTC change over development, we visualized the white matter connections of all category-selective fROIs in all participants. Fig 4 shows an example infant at newborn, 3 months, and 6 months as well as an example adult (connections of all participants in Supplementary Figs 12-50).

Consistent with the prior analyses, within an age group, white matter connections of fROIs in the same cytoarchitectonic area were similar. For example, in the newborn, pFus-faces and pOTS-words, both in FG2, are characterized by vertical connections to dorsal occipital cortex and longitudinal connections to both the anterior temporal lobe and early visual cortex (Fig 3A, top 2 rows). However, we also observe developmental changes. For example, pFus-faces and pOTS-words appear to have more abundant vertical connections in infants than adults, but more connections to the frontal cortex in adults than infants (Fig 3A, Supplementary Figs 20-27, 47-50 all participants). We see a similar pattern for the white matter connections of fROIs in FG4: mFus-faces, OTS-bodies, and OTS-words show similar connectivity profiles at each timepoint (e.g., newborn), yet we also observe developmental differences: vertical connections appear more abundant in newborns than adults, but connections to the frontal cortex appear to be more abundant in adults than infants (Fig 3A, bottom row, Supplementary Figs 12-19, 28-35,44-46). For CoS-places, located medially in FG3, there is a different connectivity profile and a different developmental pattern: in newborns, CoS-places has abundant frontal, vertical, and longitudinal connections to both occipital and anterior temporal lobes, but in adults there appear to be fewer frontal and vertical connections (Fig 3A-third row, Supplementary Figs 36-43).

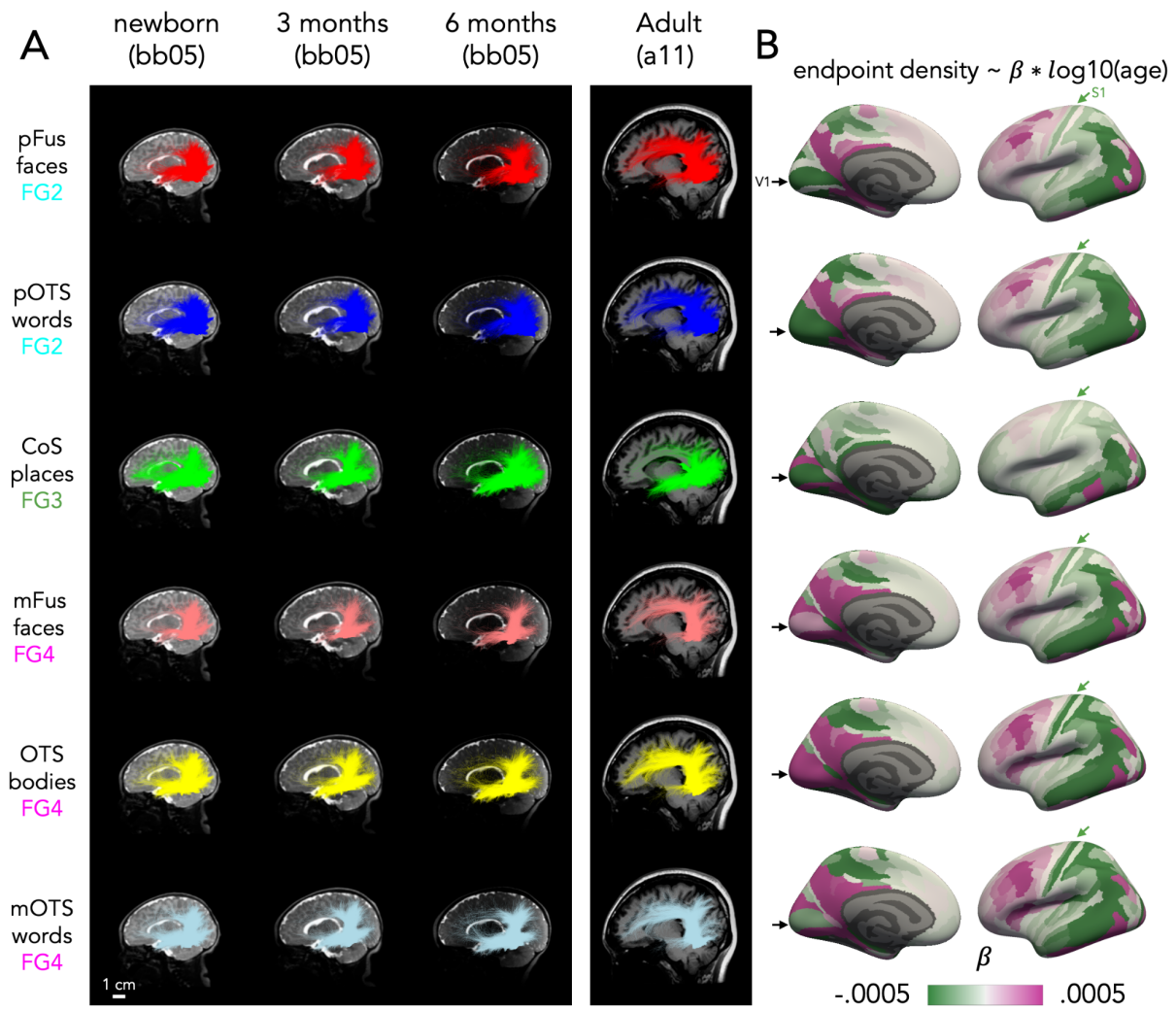

Figure 4. Connectivity of VTC develops from infancy to adulthood . (A) Connections of each category-selective ROI in an individual infant (bb05) across three time points (newborn, 3 months, 6 months) next to an adult control (A11) shown in a sagittal cross section. Brains are shown to scale, see scale bar bottom left. Each row is a different fROI (indicated by color) and ordered by cytoarchitectonic area, from top to bottom: FG2 to FG4. (B) Change in endpoint density over development for each fROI's connectivity profile. The color of the Glasser ROI indicates the development in endpoint density over time, namely the slope of the regression: endpoint density ~ log10(age in days) for 88 sessions. Here we report data for the left hemisphere because it includes all 6 fROIs. Data for the right hemisphere is in Supplementary Fig 51. *Green*: decreasing endpoint density over development, *magenta:* increasing endpoint density over development. *Black arrow: primary visual area* (V1), *Green arrow:* primary somatosensory area(S1). Each row shows the development of white matter connections of an fROI; rows are ordered identically to (A).

To quantify developmental changes, we test whether each fROI's endpoint density, quantified as the proportion of connections in each Glasser ROI, varies as a function of age (fROI endpoint density ~ log10(age in days) x Glasser ROI, linear model). As expected, fROIs' endpoint density vary across the brain (significant main effect of Glasser ROI; $Fs > 3.54$, $ps < 2.2\text{x}10^{-16}$; statistics in Supplementary Table 1) reflecting that fROIs have non-uniform connectivity across the brain.

Additionally, fROIs' endpoint density differentially vary with age across the brain (significant age by Glasser ROI interaction; *F*s > 74.94, *p*s < 2.2×10^{-16}; statistics in Supplementary Table 1). As we find a differential development across the brain, for each fROI, we calculate the change in endpoint density across age per Glasser ROI (endpoint density ~ log10(age in days), linear model). Then, we visualize the slope of this model for each Glasser ROI (Fig 4D). A positive slope (magenta) indicates that the endpoint density increases from infancy to adulthood within the Glasser ROI, whereas a negative slope (green) indicates that endpoint density decreases with age. This analysis reveals both developmental increases and decreases in endpoint density with distinct spatial characteristics. First, there are common developmental patterns for face, word, and body fROIs (Fig 4-right): endpoint densities to lateral occipital and dorsal occipito-parietal visual Glasser ROIs as well as somatosensory areas decrease (Fig 4-green arrows), but endpoint densities to lateral prefrontal Glasser ROIs increase (Fig 4). There are also differential developmental patterns of connectivities of fROIs in FG2 (pOTS-words, pFus-faces) compared to FG4 (mFus-faces mOTS-words, and OTS-bodies): the former show developmental decreases in endpoint densities in V1 and early visual cortex more broadly (Fig 4-medial view) but the latter show developmental increases. Finally, for CoS-places, which is in FG3, we find mostly developmental decreases in endpoint densities in both visual and orbitofrontal cortex with increases in endpoint densities in ventral temporal lateral regions.

Finally, we test whether development was more similar for fROIs with the same cytoarchitectonic area or same category-selectivity. We use a bootstrapping procedure to estimate the developmental slopes (see Methods), and evaluate the similarity between white matter development by calculating the pairwise correlation between the development slopes across Glasser ROI for each pair of fROIs. We then fit a linear model to test whether the correlation was higher for fROIs with the same cytoarchitecture or category-selectivity (linear model: Fisher Transformed correlation ~ cytoarchitecture + category). We find a significant main effect of cytoarchitecture ($F(1,14997) = 61{,}161.5$, $p < 2.2 \times 10^{-16}$), reflecting that regions within the same cytoarchitectonic area had more similar developmental slopes (correlation$\pm$sd: .78$\pm$11) than regions in different cytoarchitectonic areas (correlation$\pm$sd: .25$\pm$13). There was also a significant main effect of category ($F(1,14997) = 1{,}069.1$ $p < 2.2 \times 10^{-16}$). However, here we find that regions with the same category-selectivity had less similar developmental slopes (correlation$\pm$sd: .36$\pm$16) than regions with different category-selectivity (correlation$\pm$sd: .40$\pm$.28). These analyses suggest that although the relationship between white matter and cytoarchitecture is consistent over development, connectivity profiles develop in parallel within each cytoarchitectonic area, with both developmental increases and decreases in endpoint densities.

Discussion

Here, we use anatomical and diffusion MRI in infants within the first six months of life and in adults to determine the organizing principles and developmental trajectories of the white matter connections of regions in VTC. We find that white matter connections are organized by cytoarchitecture, eccentricity, and category from birth. We also find evidence for development of white matter connections of VTC, with increasing endpoint density to lateral frontal cortex, and decreasing endpoint density to lateral occipital, parietal, somatosensory, and orbitofrontal cortex. These findings have important implications for understanding the interplay between nature and nurture on both white matter connections and functional brain development.

Innate aspects of white matter connections of VTC: cytoarchitecture and eccentricity are parsimonious principles

A predominant theory suggests that the consistent organization of category-selective regions in VTC is due to innate white matter connections that support category-specific processing[11,12,15,26]. While we find that in infancy white matter connections are organized to a certain extent by category, especially for faces and places, several of our empirical findings suggest that cytoarchitecture and eccentricity are more parsimonious organizing principles of white matter connectivity from infancy to adulthood. Even as both category and cytoarchitecture can be classified from whole brain white matter connectivity profiles irrespective of age, classification of cytoarchitecture is higher than category-selectivity. In addition, the subset of connections betweenVTC and early visual cortex are organized topographically by eccentricity bands and show similar eccentricity biases for functional regions that are selective for different categories but located in the same cytoarchitectonic area. Finally, connectivity profiles of functional regions in the same cytoarchitectonic area largely develop in parallel from infancy to adulthood. This organization by cytoarchitecture and eccentricity suggests that these are general principles underlying the white matter organization of the visual system, which may predate and constrain the coupling of white matter connections and brain function. That is, our data suggest a theoretical shift: rather than humans being born with specialized connections to support category-specific processing, there may be more general principles underlying the white matter organization of the visual system that correspond to cytoarchitectonic boundaries and eccentricity gradients. Indeed, in children and adults cytoarchitecture and eccentricity are linked as the boundary between lateral and medial cytoarchitectonic areas in VTC align to the transition between foveal and peripheral representations in VTC[20,52,55,56].

As cytoarchitectonic[30,53,57–60] and retinotopic organization[7,8,21,61–63] are prevalent across the entire visual system, we hypothesize that these two organizing principles may underlie the white matter organization of the visual system more broadly. This hypothesis can be tested in future research, for example, in the parietal cortex that contains a series of retinotopic[64,65] and cytoarchitectonic[58] areas. Critically, as cytoarchitecture[30,54,6630,67–70], and topography[71,72] are also key features distinguishing brain areas beyond the visual system, e.g., language[73], our findings raise the

possibility that white matter connections are innately organized by cytoarchitecture and topographic gradients even beyond the visual system and throughout the entire brain. This hypothesis can be tested in future research leveraging large anatomical and diffusion MRI datasets that are being collected in infants[74–78].

Development of white matter connections of VTC

While we find innate organization of white matter connections, we also find that the connectivity profiles of fROIs within the same cytoarchitectonic area develop in parallel from infancy to adulthood. Endpoint density from VTC to the frontal lobe showed both developmental increases and decreases. Endpoint density from FG2 and FG4 in lateral VTC to prefrontal cortex increased over development but from FG3 in medial VTC to orbitofrontal cortex decreased. The former finding is consistent with observations that the arcuate fasciculus[79] is underdeveloped in infants, only reaching the precentral gyrus and premotor cortex in newborns, and not reaching lateral prefrontal cortex as it does in adults[45,80].

Additionally, we find developmental decreases in endpoint density between VTC and lateral occipital, parietal, and somatosensory cortex. Our observations in the human visual system mirror results from a large body of tracer studies in cats and macaques that documented exuberant connections between V1, V2, and V3[81–83] as well as between early visual areas and somatosensory areas[84]. These exuberant connections are present early in development and then eliminated by adulthood[82,84–86]. Our data not only suggest that exuberant connections may exist in the human visual system, but also suggest the possibility that connections between VTC and both the lateral and dorsal visual streams[17,87–90] may decrease over development.

We acknowledge that our *in-vivo* dMRI measurements do not enable us to make inferences about the cellular and molecular underpinnings of the development of white matter connectivity profiles. However, our findings provide new ideas that can be investigated in future histological and animal research. Future studies can examine if developmental increases in endpoint density may be related to increased myelination[91–94], axonal sprouting[95–97], and glial proliferation[92,94] that are associated with activity-dependent white matter plasticity[98,99]. In addition, it can be tested whether developmental decreases in endpoint density may be related to elimination of exuberant long range projections[82,84–86].

Implications for theories of functional development of VTC

Several theories have posited that innate white matter connections of VTC constrain its function[13–15]. Here, we provide support for these theories by showing that the main principles of white matter organization persist from infancy to adulthood. At the same time, new questions regarding the functional development of VTC emerge from our findings.

First, our data demonstrate that anatomical locations corresponding to adult face and place-selective regions already have distinct whole brain connections at birth. This finding suggests that white matter connections are already organized by category at birth. Questions for future studies will be at what age face and place-selective regions first appear and whether they emerge in a stable anatomical location from infancy to adulthood, as predicted by the white matter.

Second, we find that white matter connections between EVC and VTC are organized by eccentricity from birth. This discovery is consistent with studies in infant human and nonhuman primates[26,33] finding stronger functional connectivity between face-selective regions and foveal V1, and place-selective regions and peripheral V1. Together, these observations suggest that white matter connectivity has functional ramifications, and lead to the prediction that eccentricity biases in VTC[7,8] will be present from birth.

Third, our findings that the white matter connections of VTC have both innate organization and the capacity to change over development raise new questions about the relationship between white matter and function in atypical development. One question is whether lack of visual experience may reshape white matter connectivity profiles of VTC and consequently function[14]. For example, it is unknown if lack of visual experience may lead to the preservation of connections between VTC and somatosensory cortex, which in turn, may enable VTC to respond to haptic inputs in individuals who are congenitally blind[100]. Critically, our framework enables measuring the fine-grained white matter connections of VTC in individual infants longitudinally[101], increasing accuracy and precision in measuring the interplay between white matter connections, functional regions, and anatomy across development. Our framework opens new opportunities not only for evaluating development of white matter associated with functional regions in large infant datasets[74–78] but also for early identification and assessment of developmental disorders associated with VTC such as autism[102–105], Williams syndrome[106], congenital prosopagnosia[107,108], and dyslexia[109,102–105].

Together, the present study advances our understanding of white matter organization in the visual system suggesting that cytoarchitecture, eccentricity, and category are organizing principles from birth, even as aspects of the white matter develop from infancy to adulthood. These data have implications not only for theories of cortical functional development, but also have ramifications for early identification of atypical white matter development.

Methods

Participants

The study was approved by the Institutional Review Board of Stanford University. Parents of the infant participants provided written informed consent before the first scan session, and also provided written informed consent prior to each session if they came for multiple sessions. Participants were paid $25/hour for participation.

Expectant parent and infant screening procedure

Expectant parents and their infants in our study were recruited from the San Francisco Bay Area using social media platforms. We performed a two-step screening process. First, parents were screened over the phone for eligibility based on exclusionary criteria designed to recruit a sample of typically developing infants. Second, eligible expectant mothers were screened once again after giving birth. Exclusionary criteria were as follows: recreational drug use during pregnancy, significant alcohol use during pregnancy (more than three instances of alcohol consumption per trimester; more than 1 drink per occasion), taking prescription medications for a disorder involving psychosis or mania during pregnancy, insufficient written and spoken English ability to understand the instructions of the study, or learning disabilities. Exclusionary criteria for infants were preterm birth (<37 gestational weeks), low birthweight (<5 lbs 8 oz), any congenital, genetic, and neurological disorders, visual problems, complications during birth that involved the infant (e.g., NICU stay), history of head trauma, and contraindications for MRI (e.g., metal implants).

44 full term infants following a typical pregnancy participated in a total of 77 MRI sessions. Four sessions were excluded for missing diffusion data, and six sessions were excluded for too much motion (see Quality Assurance section). We report data from 42 infants over 67 sessions (21 longitudinal): sex: 16 female, 26 male; race and ethnicity: 4 Asian, 5 Hispanic, 11 Multiracial, and 22 White participants; age: n=23 newborns (M=28.56 days, SD= 10.21days), n=23 3-month-olds (M=106.91 days, SD=19.33 days), and n=21 6-month-olds (M=189.05 days, SD=15.77 days).

We also collected data from 21 adults: sex: 17 female, 4 male; race and ethnicity: 12 Asian, 1 Hispanic, 2 Multiracial, and 6 White participants; age: M=28.21 years, SD=5.51 years. All adult sessions met inclusion criteria.

MRI acquisitions

Scanning sessions were scheduled in the evenings around the infants' typical bedtime and were done during natural sleep. Experimenters waited till the infant fell asleep to place the infant in the MRI scanner and start the session. Infant data were acquired on a 3T GE Ultra High Performance

(UHP) scanner (GE Healthcare, Waukesha, WI) equipped with a customized 32-channel infant head-coil [110].

Hearing protection included soft wax earplugs inserted to the infant's ears and then, MRI compatible neonatal noise attenuators (https://newborncare.natus.com/products-services/newborn-care-products/nursery-essentials/minimuffs-neonatal-noise-attenuators), and headphones. (https://www.alpinehearingprotection.com/products/muffy-baby) that covered the infant's ears. During sessions with newborns, an MR-safe plastic immobilizer (MedVac, www.supertechx-ray.com) was used to stabilize the infant and their head position. When the infant was asleep, the caregiver placed the infant on the scanner bed. Weighted bags were placed at the edges of the bed to prevent any side-to-side movement. Additional pads were also placed around the infant's head and body to stabilize head position. An experimenter stayed inside the MR suite with the infant during the entire scan.

For additional monitoring of the infant's safety and tracking of the infant's head motion, an infrared camera was affixed to the head coil and positioned for viewing the infant's face in the scanner. The researcher operating the scanner monitored the infant via the camera feed, which allowed for the scan to be stopped immediately if the infant showed signs of waking or distress. This setup also allowed tracking the infant's motion; scans were stopped and repeated if there was excessive head motion.

Anatomical MRI acquisition

We obtained both T1-weighted and T2-weighted MRI data for each infant and session with the following parameters: T1-weighted image: TE = 2.9ms; TR = 6.9ms; voxel size = 0.8x 0.8 x0.8 [$mm^{3]}$; FOV = 20.5 cm; Scan time: 3:05 min; T2-weighted image: TE = 124ms; TR = 3650 ms; voxel size = 0.8x 0.8x 0.8 [$mm^{3]}$; FOV = 20.5 cm; Scan time: 4:05 min.

Anatomical MRI processing

The T1-weighted and T2-weighted images from each individual were first aligned with each other, then aligned to a plane running through the commissures (AC-PC transformed), and then processed with iBEAT V2.0[111] tissue segmentation. White matter segmentation was, and then manually fixed for errors using ITKgray[112]. We used the manually edited segmentation file to reconstruct the cortical surface with Infant FreeSurfer[113].

Diffusion MRI (dMRI) acquisition

We obtained dMRI data with the following parameters: multi-shell, #diffusion directions/b-value = 9/0, 30/700, 64/2000; TE = 75.7 ms; TR = 2800 ms; voxel size = 2x2x2 mm^3; number of slices = 60; FOV = 20 cm; in-plane/through-plane acceleration = 1/3; scan time: 5:08 min. We also

577 acquired a short dMRI scan with reverse phase encoding direction and only 6 b = 0 images (scan
578 time 0:20 min).

579 *Diffusion MRI processing*

580 The dMRI data were preprocessed using MRtrix3[114] (https://github.com/MRtrix3/mrtrix3) and in
581 accordance with prior work from the human connectome project and our lab [40,115,116]. Data were
582 denoised using principal component analysis[117]. We used FSL's top-up tool
583 (https://fsl.fmrib.ox.ac.uk/) and one image with reverse phase-encoding to correct for
584 susceptibility-induced distortions. We used FSL's eddy tool to perform eddy current and motion
585 correction, where outlier slices were detected and replaced[118]. Finally we performed bias correction
586 using ANTs[119] (https://picsl.upenn.edu/software/ants/). The preprocessed dMRI data were aligned
587 to the T2 weighted anatomy using whole-brain rigid body registration. Alignment was checked
588 manually for all images.

589 *Generating White Matter Connectomes*

590 We generated a whole brain white matter connectome in each session using MRTrix3[114]. Voxel-
591 wise fiber orientation distributions (FODs) were calculated using constrained spherical
592 deconvolution (CSD). We used the Dhollander algorithm[120] to estimate the three-tissue response
593 function. We lowered the FA threshold to 0.1 to account for the generally lower FA in infant brains.
594 We computed FODs separately for the white matter and CSF. As in past work[40,115], the gray matter
595 was not modeled separately, as white and gray matter do not have sufficiently distinct b-value
596 dependencies to allow for a clean separation of the signals. Finally, we generated a whole brain
597 white matter connectome for each session. Tractography was optimized using the gray/white
598 matter segmentation from anatomical MRI data (Anatomically Constrained Tractography; ACT[121]).
599 For each connectome, we used probabilistic fiber tracking with the following parameters: IFOD2
600 algorithm, step size of 0.2 mm, minimum length of 4 mm, maximum length of 200 mm, and
601 maximum angle of 15°. Streamlines were randomly seeded on this gray-matter/white-matter
602 interface, and each connectome consisted of 5 million streamlines. This procedure is critical for
603 accurately identifying the connections that reach fROIs, which are located in the gray matter[122].

604 *Quality Assurance*

605 To evaluate the quality of the diffusion data we implemented three quality assurance measures: (i)
606 We measured the number of outliers (dMRI volumes with signal dropout measured by FSL's eddy
607 tool). The exclusion criterion was >5% outlier volumes as in past work[20]. (ii) We visualized in mrView
608 the fractional anisotropy (FA) colored by direction of the diffusion tensors to validate the expected
609 maps. That is, the existence of between hemispheric connections through the corpus callosum,
610 and the inferior-superior directionality of the cerebral spinal tract.(iii) We used babyAFQ[22] to identify

611 the bundles of the brain and validate that the major bundles known to be present at birth[40,41,123] can
612 be found in each individual and session.

613 These quality assurance measures lead to the following data exclusions:

614 (i) No adult sessions were excluded for outliers. Six infant sessions were excluded because they
615 had >5% outliers. After exclusion, there were no significant differences in outlier volumes between
616 the infants and the adults (infants: mean percent outliers±SD = 0.45% ± 0.43%; adults: mean percent
617 outliers±SD = 0.29% ± 0.10%; $t(86) = 1.70$, $p = .092$).

618 (ii) We identified the corpus callosum with left-right directionality and corticospinal tract with
619 inferior-superior directionality in all infant and adult sessions, so no data was excluded due to this
620 measure.

621 (iii) Using babyAFQ, we identified the major bundles in the infant brain and using AFQ, we identified
622 these bundles in adults. In each infant and adult session we identified the arcuate (AF), posterior
623 arcuate (pAF), vertical occipital (VOF), inferior longitudinal (ILF), superior longitudinal (SLF),
624 corticospinal (CST), cingulate (CC), forceps major (FcMa), and forceps minor (FcMi), as such no
625 data were excluded. This confirms the quality of dMRI data and our tracking procedure as we could
626 identify the major white matter bundles that are known to exist from birth in all sessions.

627 *Cytoarchitectonic Areas of VTC*

628 We used the Rosenke Atlas[53] that contains maximum probability maps (MPMs) of 8
629 cytoarchitectonic regions of the human ventral visual stream, created from 10 post mortem adult
630 samples published in[32,124]. We used cortex based alignment in FreeSurfer[51] (https://freesurfer.net/,
631 mri_label2label) to map the MPM of four cytoarchitectonic areas of the ventral stream FG1, FG2,
632 FG3, FG4 to each cortical surface for each of the 88 sessions in the study. Two independent raters
633 (SD, DO) manually checked each brain to examine if the mid fusiform sulcus (MFS) was the
634 boundary between FG3/FG4 and FG1/FG2 as reported in prior studies[5,52]. In places where there
635 were disagreements between the raters, alignment was checked by KGS. The analysis confirmed
636 that the boundaries between the cytoarchitectonic areas aligned with the MFS (see examples in
637 Fig 1c) except for five infants in the right hemisphere, and one adult in the left hemisphere.

638 *Category-Selective Regions of VTC*

639 A functional atlas of category-selective regions of VTC was created from independent fMRI data in
640 28 adults from a previously published study[20]. Participants included 11 females and 17 males ages
641 22.1–28.6 years, (mean±SD = 24.1±1.6 years. Category-selective regions were defined in each of
642 the 28 individuals using the fLoc experiment containing low-level and familiarity-controlled gray

643 level images of items from 10 visual categories[125]. Category-selective regions were defined using
644 a voxel-level t-statistic contrasting each category of interest with all other categories (t > 3, no
645 spatial smoothing), and anatomical criteria[5,6,125]. We defined two face-selective regions on the
646 fusiform gyrus of each hemisphere, mFus-faces and pFus-faces using the contrast of (faces >
647 bodies, limbs, characters, objects, places). We defined OTS-bodies in both hemispheres as the
648 region on the occipital temporal sulcus selective for bodies (bodies and limbs > characters, faces,
649 objects, places). We defined CoS-places in both hemispheres as the region in the intersection
650 between the collateral sulcus (CoS) and anterior lingual sulcus (ALS) that was selective for places
651 (places > faces, characters, objects, bodies, limbs). Finally, we identified mOTS-words and pOTS-
652 words as the regions in the occipital temporal sulcus (OTS) that were selective for words
653 (psuedowords > faces, scenes, objects, bodies, limbs). After identifying the functional regions
654 within each participant we mapped the regions to the fsaverage template brain space using cortex
655 based alignment[51]. We then created probabilistic maps for each fROI where each vertex was the
656 probability of a participant having the fROI at that location (a value of 1 meant that all participants
657 had the region at that location and a value of .5 meant that half of participants had a value at that
658 location). We thresholded the probabilistic maps at .2 and then created MPMs, where in the case
659 that two fROIs had probabilistic values > .2 at the same vertex, the vertex was assigned to the fROI
660 with the highest probability (as in[126]). MPM-fROIs of word-selective regions were only found in the
661 left hemisphere due to their left lateralization[127,128].

662 To map fROIs to individual participants' cortical space for the 88 sessions of the main experiment,
663 we used cortex based alignment in Freesurfer[51] (https://freesurfer.net/, mri_label2label). Two
664 independent raters (DO and SD) then visually checked each surface to ensure that the fROIs were
665 aligned to the expected anatomical landmarks in each individual participant. Specifically, the raters
666 checked whether mFus-faces aligned to the mid fusiform sulcus (MFS) and whether CoS-places
667 aligned to the junction of the ALS and CoS. When there was disagreement, KGS then checked
668 whether the fROIs aligned to anatomical landmarks. Category-selective fROIs aligned to these
669 anatomical landmarks in all hemisphere except for one infant in which left hemisphere CoS-places
670 did not align to the junction or the ALS and CoS, and two infants in which right hemisphere mFus-
671 faces did not align to the MFS. We show the mapping of each fROI in each participant in
672 Supplementary Figs. 1-8.

673 We tested whether there were size differences in how the fROIs mapped to each individual brain.
674 To do so, tested if fROI surface area relative to brain surface varied with age:

675 (1) (fROI surface area)/(brain surface area) ~ log10(age in days).

676 We found no significant differences between infants and adults on fROI surface area relative to
677 brain surface area (effect of age: $t(878) = 8.77 \times 10^{-6}$, $p = 0.88$)), reflecting that fROIs were the same
678 size relative to the size of the brain regardless of age.

Identifying functionally defined white matter connections

To identify the white matter connections of each fROI, we intersected the whole brain connectome generated from dMRI and tractography in each participant. We used an open source software package, FSuB-Extractor[101] (https://github.com/smeisler/fsub_extractor) to intersect each fROI with the whole brain connectome of each participant and identify the white matter connections of the fROI. In brief, the software takes in fROIs in the native space of each participant and projects them along the surface normal into the gray-matter-white-matter interface. It then restricts the fROI to the gray-matter-white-matter interface and then selects all streamlines that intersect with the fROI.

Defining connectivity profiles

For each fROI, we define its connectivity profile or how it connects to the rest of the brain. To do so, we took the white matter connections of each fROI (see above), projected their endpoints to the cortical surface using tract density imaging (TDI) with mrTrix3[114], and calculated the distribution of these white matter endpoints across all cortical surface vertices. We transformed the TDI output into a distribution of endpoints by dividing the endpoint map by the total number of endpoints. This results in an endpoint density map that sums to 1 for each fROI and participant. We then used the Glasser Atlas[54] to quantify how the endpoints were distributed across the brain. We chose to use the Glasser Atlas because it covers the whole cortical surface of each hemisphere, and because it divides cortex into meaningful parcellations according to functional and anatomical criteria. For each fROI, we define the white matter connectivity profile or the endpoint density in each region in the Glasser Atlas. The Glasser Atlas consists of 180 regions per hemisphere. As in prior work[20], we excluded 11 VTC regions of the Glasser Atlas to avoid quantifying looping fibers from the seed fROI. Therefore, each connectivity profile consisted of the endpoint density across 169 regions in the Glasser Atlas within the same hemisphere of the fROI.

Principal Components Analysis

Because our connectivity profiles are high-dimensional (169), we used principal component analysis (PCA) to reduce the dimensionality of the connectivity profiles. We conducted PCA on the 880 (10 fROIs x 88 sessions connectivity profiles) x 169 (Glasser ROIs) endpoint connectivity matrix. We used find_curve_elbow in R (https://rdrr.io/cran/pathviewr/man/find_curve_elbow.html) to find the elbow of the curve of principal components vs variance explained and found that the first 10 principal components explained 98% of the variance in the data. In Figure 2, we plot the first principal component (explains 38% of the variance) vs the second principal component (explains 20% of the variance). Each dot represents a single connectivity profile in a single subject and session; The connectivity profiles (dots) can be coded by different features (the cytoarchitectonic area, category-preference, or participant's age).

Classification of Cytoarchitecture, Category and Age from Connectivity Profile

We used a n-way leave-one-out classifier to test if we could predict different features (cytoarchitecture, category, or age) of a held-out connectivity profile. For each feature (cytoarchitecture, category, age), we used multinomial logistic regression (fit on all data except for the held out subject) to predict the feature of the held out connectivity profile (e.g., probability of belonging to FG2, FG3, or FG4 for the cytoarchitecture classification). We used a winner-take-all approach and assigned the connectivity profile to the label with the highest probability. We repeated the process for each connectivity profile (leave-one-out cross-validation). We then calculated classification accuracy by comparing the predicted classification to the ground truth. We performed three separate classifications: one predicting cytoarchitecture (FG2/FG3/FG4), one predicting category (face/word/body/place), and one predicting age group: (newborn/3 months/6 months/adult). Additionally, we performed separate classifications predicting category (face/word/body/place) and age group (newborn/3 months/6 months/adults) within each cytoarchitectonic area.

Connections to Eccentricity Bands in Early Visual Cortex

To test how each fROI connects to different eccentricity bands in early visual cortex (EVC), we created a region of interest corresponding to EVC from the union of V1, V2, and V3 ROIs from the Benson Atlas[129]. We then used the average retinotopic map in 21 adults from a previously published paper[130] to divide the EVC fROI into three eccentricity bands, 0-5°, 5-10°, and 10-20°. Using cortex based alignment in FreeSurfer (mri_label2label) we aligned each of these EVC eccentricity band ROIs to each individual participant's native space. We then used FSuB-Extractor [101] (https://github.com/smeisler/fsub_extractor), to identify the white matter connections between each fROI and each eccentricity band in VTC. We divided the number of streamlines connecting to each eccentricity band by the total number of streamlines between the fROI and EVC to estimate the percentage of streamlines connected to each eccentricity band. To test if the percentage of streamlines to each eccentricity band differs by cytoarchitecture, category, and age, we fit the following model:

(2) percentage of streamlines in central 5° ~ cytoarchitecture x category x age group

After finding a significant cytoarchitecture by category interaction, we performed post-hoc tests to determine which fROIs were driving the interaction. To do so, we used paired t-tests to test whether the percentage of streamlines in the central 5° differed for fROIs within the same cytoarchitectonic area for the following pairs of fROIs: pFus-faces and pOTS-words in FG2, mFus-faces and OTS-bodies in FG4, mFus-faces and mOTS-words in FG4, and OTS-bodies and mOTS-words in FG4.

After finding a significant cytoarchitecture by age interaction, we performed post-hoc tests to test whether the percentage of streamlines in the central 5° differed as a function of age for fROIs within

each cytoarchitectonic area using the following model separately for each cytoarchitectonic area (FG2, FG3, FG4):

(3) percentage of streamlines in central 5° ~ log10(age) + (1|subject)

After finding a significant interaction between cytoarchitecture, category, and age we performed post-hoc tests to test whether the percentage of streamlines to the central 5° changed over development using the following model separately for each fROI (pFus-faces, pOTS-words, CoS-places, mFus-faces, OTS-bodies, mOTS-words):

(4) percentage of streamlines in central 5° ~ log10(age) + (1|subject)

Quantifying development

As development is expected to asymptote across the lifespan and typically follows a logarithmic function of age, to quantify how white matter connectivity profiles change with age, we fit a linear model predicting endpoint density of each fROI as a function of Glasser ROI and log10(age in days) across the brain. Age is a continuous variable and Glasser ROI is a categorical variable. As endpoint density was normalized to sum to one across the brain, it is not appropriate to model a random intercept for each subject.

(5) fROI endpoint density ~ log10(age in days)xGlasser ROI

After finding a significant Glasser ROI by age interaction (Supplementary Table 4), for each fROI, we fit linear models relating endpoint density vs log10(age) separately for each Glasser ROI to quantify the development of endpoint density within each Glasser ROI. The regression slope quantifies the rate of the development:

(6) fROI endpoint density ~ log10(age in days).

We visualize the regression results in Fig 4B, where each Glasser ROI is colored by the slope of the regression. Data is reported for the left hemisphere in the main text and Fig 3 because all 6 fROIs are found consistently in the left hemisphere. Data from 4 fROIs in the right hemisphere is reported in Supplementary Figure 53. Supplementary Tables 2-7 provide all the developmental slopes per Glasser ROI.

Calculating the similarity between developmental slopes

To test whether development was more similar for regions within the same cytoarchitectonic area or category-selectivity we estimated the similarity between developmental slopes of white matter connectivity of fROI pairs using a bootstrapping procedure.

First, we calculated the developmental slopes of endpoint connectivity across the brain using a bootstrapping procedure. For each fROI, and for each of 1000 iterations we used 75% of the data (66 randomly selected connectivity profiles), and calculated the developmental slope within each of the 169 Glasser ROIs using the following model:

(7) fROI endpoint density ~ log10(age in days)

Then for each pair of fROIs we calculated the pairwise correlation between the vector of 169 slopes across the bootstrap iterations. Finally, we fit a linear model to test whether the Fisher transformed correlation between development slopes was higher for fROIs with the same cytoarchitecture and category-selectivity than for fROIs with different cytoarchitecture and category-selectivity. We calculated the Fisher transform to ensure normality (as correlations are bounded between -1 and 1); category and cytoarchitecture are categorical variables (same: 1; different: 0).

(8) FisherZ(correlation) ~ category + cytoarchitecture

Data availability

The data to make the figures, tables, and statistics associated with this manuscript is available here: https://github.com/VPNL/bbVTCwm/tree/main/data

Code availability

The code to analyze the data, compute statistics, and make the individual figure elements is available here: https://github.com/VPNL/bbVTCwm/. The code folder contains the R code used to generate all other figures and statistics in the figures/ and statistics/ subdirectories. The code used to preprocess the data and perform the analyses are included in the analyses/ subdirectory. The label files for the fROIs and the EVC ROIs are provided in the labels folder. The supplement folder contains code to generate Supplementary Figures.

Author Contributions

EK: designed the analyses, wrote the code and data analysis pipelines, analyzed the data, and wrote the manuscript. XY: participated in the design and data analysis, and collected the data. ST, BF, CT collected the data, segmented each brain anatomy image into gray and white matter and created cortical surface reconstructions. SF and DO: validated the alignment between fROIs, cytoarchitectonic areas and anatomical landmarks. MG: participated in the data analyses. VSN: participated in the design and data analysis, and collected the data. BK: designed the infant coil used for data collection. KGS: oversaw all parts of the research: design, data analysis, and wrote the manuscript. All authors read and gave feedback on the manuscript.

Acknowledgements

This work was funded by Stanford Wu Tsai Neurodevelopment big idea and accelerator grants, as well as NIH grants R01EY033835 and R01EY022318 to KGS. EK was supported by the National Science Foundation Graduate Research Fellowship (grant number DGE-1656518); MG was funded by the Deutsche Forschungsgemeinschaft (DFG, German Research Foundation – project number 222641018 – SFB/TRR 135 TP C10), as well as by "The Adaptive Mind", funded by the Excellence Program of the Hessian Ministry of Higher Education, Science, Research and Art.

References

1. Kanwisher, N., McDermott, J. & Chun, M. M. The fusiform face area: a module in human extrastriate cortex specialized for face perception. *J. Neurosci.* **17**, 4302–4311 (1997).
2. Peelen, M. V. & Downing, P. E. Selectivity for the human body in the fusiform gyrus. *J. Neurophysiol.* **93**, 603–608 (2005).
3. Cohen, L. *et al.* Language-specific tuning of visual cortex? Functional properties of the Visual Word Form Area. *Brain* **125**, 1054–1069 (2002).
4. Epstein, R., Harris, A., Stanley, D. & Kanwisher, N. The parahippocampal place area: recognition, navigation, or encoding? *Neuron* **23**, 115–125 (1999).
5. Weiner, K. S. *et al.* The mid-fusiform sulcus: a landmark identifying both cytoarchitectonic and functional divisions of human ventral temporal cortex. *Neuroimage* **84**, 453–465 (2014).
6. Weiner, K. S. *et al.* Defining the most probable location of the parahippocampal place area using cortex-based alignment and cross-validation. *Neuroimage* **170**, 373–384 (2018).
7. Levy, I., Hasson, U., Avidan, G., Hendler, T. & Malach, R. Center–periphery organization of human object areas. *Nat. Neurosci.* **4**, 533–539 (2001).
8. Hasson, U., Levy, I., Behrmann, M., Hendler, T. & Malach, R. Eccentricity Bias as an Organizing Principle for Human High-Order Object Areas. *Neuron* **34**, 479–490 (2002).
9. Natu, V. S. *et al.* Infants' cortex undergoes microstructural growth coupled with myelination during development. *Commun Biol* **4**, 1191 (2021).

10. Cachia, A. *et al.* How interindividual differences in brain anatomy shape reading accuracy. *Brain Struct. Funct.* **223**, 701–712 (2018).

11. Saygin, Z. M. *et al.* Anatomical connectivity patterns predict face selectivity in the fusiform gyrus. *Nat. Neurosci.* **15**, 321–327 (2011).

12. Osher, D. E. *et al.* Structural Connectivity Fingerprints Predict Cortical Selectivity for Multiple Visual Categories across Cortex. *Cereb. Cortex* **26 4**, 1668–1683 (2016).

13. Saygin, Z. M. *et al.* Connectivity precedes function in the development of the visual word form area. *Nat. Neurosci.* **19**, 1250–1255 (2016).

14. Bi, Y., Wang, X. & Caramazza, A. Object Domain and Modality in the Ventral Visual Pathway. *Trends Cogn. Sci.* **20**, 282–290 (2016).

15. Mahon, B. Z. & Caramazza, A. What drives the organization of object knowledge in the brain? *Trends Cogn. Sci.* **15**, 97–103 (2011).

16. Kanwisher, N. Functional specificity in the human brain: a window into the functional architecture of the mind. *Proc. Natl. Acad. Sci. U. S. A.* **107**, 11163–11170 (2010).

17. Weiner, K. S., Yeatman, J. D. & Wandell, B. A. The posterior arcuate fasciculus and the vertical occipital fasciculus. *Cortex* **97**, 274–276 (2017).

18. Caffarra, S., Karipidis, I. I., Yablonski, M. & Yeatman, J. D. Anatomy and physiology of word-selective visual cortex: from visual features to lexical processing. *Brain Struct. Funct.* **226**, 3051–3065 (2021).

19. Lerma-Usabiaga, G., Carreiras, M. & Paz-Alonso, P. M. Converging evidence for functional and structural segregation within the left ventral occipitotemporal cortex in reading. *Proceedings of the National Academy of Sciences* **115**, E9981–E9990 (2018).

20. Kubota, E. *et al.* White matter connections of high-level visual areas predict cytoarchitecture better than category-selectivity in childhood, but not adulthood. *Cereb. Cortex* **33**, 2485–2506 (2023).

21. Finzi, D. *et al.* Differential spatial computations in ventral and lateral face-selective regions are scaffolded by structural connections. *Nat. Commun.* **12**, (2021).

22. Grotheer, M., Yeatman, J. & Grill-Spector, K. White matter fascicles and cortical microstructure predict reading-related responses in human ventral temporal cortex. *Neuroimage* **227**, 117669 (2021).

23. Hannagan, T., Amedi, A., Cohen, L., Dehaene-Lambertz, G. & Dehaene, S. Origins of the specialization for letters and numbers in ventral occipitotemporal cortex. *Trends Cogn. Sci.* **19**, 374–382 (2015).

24. Op de Beeck, H. P., Pillet, I. & Ritchie, J. B. Factors Determining Where Category-Selective Areas Emerge in Visual Cortex. *Trends Cogn. Sci.* **23**, 784–797 (2019).

25. Osher, D. E. *et al.* Structural Connectivity Fingerprints Predict Cortical Selectivity for Multiple Visual Categories across Cortex. *Cereb. Cortex* **26**, 1668–1683 (2016).

26. Li, J., Osher, D. E., Hansen, H. A. & Saygin, Z. M. Innate connectivity patterns drive the development of the visual word form area. *Sci. Rep.* **10**, 18039 (2020).

27. Kamps, F. S., Hendrix, C. L., Brennan, P. A. & Dilks, D. D. Connectivity at the origins of domain specificity in the cortical face and place networks. *Proceedings of the National Academy of Sciences* **117**, 6163–6169 (2020).

28. Zeki, S. & Shipp, S. The functional logic of cortical connections. *Nature* **335**, 311–317 (1988).

29. Van Essen, D. C., Anderson, C. H. & Felleman, D. J. Information processing in the primate visual system: an integrated systems perspective. *Science* **255**, 419–423 (1992).

30. Amunts, K. & Zilles, K. Architectonic Mapping of the Human Brain beyond Brodmann. *Neuron* **88**, 1086–1107 (2015).

31. Caspers, J. *et al.* Cytoarchitectonical analysis and probabilistic mapping of two extrastriate areas of the human posterior fusiform gyrus. *Brain Struct. Funct.* **218**, 511–526 (2012).

32. Lorenz, S. *et al.* Two New Cytoarchitectonic Areas on the Human Mid-Fusiform Gyrus. *Cereb. Cortex* **27**, 373–385 (2017).

33. Gomez, J., Natu, V. S., Jeska, B., Barnett, M. & Grill-Spector, K. Development differentially sculpts receptive fields across early and high-level human visual cortex. *Nat. Commun.* **9**, (2018).

34. Ellis, C. T. *et al.* Retinotopic organization of visual cortex in human infants. *Neuron* **109**, 2616–2626.e6 (2021).

35. Butt, O. H., Benson, N. C., Datta, R. & Aguirre, G. K. The fine-scale functional correlation of striate cortex in sighted and blind people. *J. Neurosci.* **33**, 16209–16219 (2013).

36. Butt, O. H., Benson, N. C., Datta, R. & Aguirre, G. K. Hierarchical and homotopic correlations of spontaneous neural activity within the visual cortex of the sighted and blind. *Front. Hum. Neurosci.* **9**, 25 (2015).

37. Arcaro, M. J. & Livingstone, M. S. A hierarchical, retinotopic proto-organization of the primate visual system at birth. *Elife* **6**, (2017).

38. Arcaro, M. J. & Livingstone, M. S. On the relationship between maps and domains in inferotemporal cortex. *Nat. Rev. Neurosci.* **22**, 573–583 (2021).

39. Dudink, J., Kerr, J. L., Paterson, K. & Counsell, S. J. Connecting the developing preterm brain. *Early Hum. Dev.* **84**, 777–782 (2008).

40. Grotheer, M. *et al.* White matter myelination during early infancy is linked to spatial gradients and myelin content at birth. *Nat. Commun.* **13**, 997 (2022).

41. Grotheer, M. *et al.* Human white matter myelinates faster in utero than ex utero. *Proc. Natl. Acad. Sci. U. S. A.* **120**, e2303491120 (2023).

42. Dubois, J., Hertz-Pannier, L., Dehaene-Lambertz, G., Cointepas, Y. & Le Bihan, D. Assessment of the early organization and maturation of infants' cerebral white matter fiber bundles: A feasibility study using quantitative diffusion tensor imaging and tractography. *Neuroimage* **30**, 1121–1132 (2006).

43. Zöllei, L., Jaimes, C., Saliba, E., Grant, P. E. & Yendiki, A. TRActs constrained by UnderLying INfant anatomy (TRACULInA): An automated probabilistic tractography tool with anatomical priors for use in the newborn brain. *Neuroimage* **199**, 1–17 (2019).

44. Dimond, D. *et al.* Early childhood development of white matter fiber density and morphology. *Neuroimage* **210**, 116552 (2020).

45. Perani, D. *et al.* Neural language networks at birth. *Proc. Natl. Acad. Sci. U. S. A.* **108**, 16056–16061 (2011).

46. Levin, N., Dumoulin, S. O., Winawer, J., Dougherty, R. F. & Wandell, B. A. Cortical maps and white matter tracts following long period of visual deprivation and retinal image restoration. *Neuron* **65**, 21–31 (2010).

47. Bauer, C. M. *et al.* Abnormal white matter tractography of visual pathways detected by high-

929 angular-resolution diffusion imaging (HARDI) corresponds to visual dysfunction in
930 cortical/cerebral visual impairment. *J. AAPOS* **18**, 398–401 (2014).

931 48. Ortibus, E. *et al.* Integrity of the inferior longitudinal fasciculus and impaired object
932 recognition in children: a diffusion tensor imaging study. *Dev. Med. Child Neurol.* **54**, 38–43
933 (2012).

934 49. Lennartsson, F., Nilsson, M., Flodmark, O. & Jacobson, L. Damage to the immature optic
935 radiation causes severe reduction of the retinal nerve fiber layer, resulting in predictable
936 visual field defects. *Invest. Ophthalmol. Vis. Sci.* **55**, 8278–8288 (2014).

937 50. Zufferey, P. D., Jin, F., Nakamura, H., Tettoni, L. & Innocenti, G. M. The role of pattern vision in
938 the development of cortico-cortical connections. *Eur. J. Neurosci.* **11**, 2669–2688 (1999).

939 51. Fischl, B., Sereno, M. I. & Dale, A. M. Cortical surface-based analysis. II: Inflation, flattening,
940 and a surface-based coordinate system. *Neuroimage* **9**, 195–207 (1999).

941 52. Weiner, K. S. *et al.* The Cytoarchitecture of Domain-specific Regions in Human High-level
942 Visual Cortex. *Cereb. Cortex* **27**, 146–161 (2016).

943 53. Rosenke, M. *et al.* A cross-validated cytoarchitectonic atlas of the human ventral visual
944 stream. *Neuroimage* **170**, 257–270 (2018).

945 54. Glasser, M. F. *et al.* A multi-modal parcellation of human cerebral cortex. *Nature* **536**, 171–
946 178 (2016).

947 55. Grill-Spector, K. & Weiner, K. S. The functional architecture of the ventral temporal cortex and
948 its role in categorization. *Nat. Rev. Neurosci.* **15**, 536–548 (2014).

949 56. Weiner, K. S. *et al.* The mid-fusiform sulcus: A landmark identifying both cytoarchitectonic
950 and functional divisions of human ventral temporal cortex. *Neuroimage* **84**, 453–465 (2014).

951 57. Caspers, S. *et al.* The human inferior parietal cortex: cytoarchitectonic parcellation and
952 interindividual variability. *Neuroimage* **33**, 430–448 (2006).

953 58. Richter, M. *et al.* Cytoarchitectonic segregation of human posterior intraparietal and adjacent
954 parieto-occipital sulcus and its relation to visuomotor and cognitive functions. *Cereb. Cortex*
955 **29**, 1305–1327 (2019).

956 59. Malikovic, A. *et al.* Cytoarchitecture of the human lateral occipital cortex: mapping of two
957 extrastriate areas hOc4la and hOc4lp. *Brain Struct. Funct.* **221**, 1877–1897 (2016).

958 60. Rottschy, C. *et al.* Ventral visual cortex in humans: Cytoarchitectonic mapping of two
959 extrastriate areas. *Hum. Brain Mapp.* **28**, (2007).

960 61. Groen, I. I. A., Dekker, T. M., Knapen, T. & Silson, E. H. Visuospatial coding as ubiquitous
961 scaffolding for human cognition. *Trends Cogn. Sci.* **26**, 81–96 (2022).

962 62. Gomez, J., Barnett, M. & Grill-Spector, K. Extensive childhood experience with Pokémon
963 suggests eccentricity drives organization of visual cortex. *Nat Hum Behav* **3**, 611–624 (2019).

964 63. Silson, E. H., Chan, A. W.-Y., Reynolds, R. C., Kravitz, D. J. & Baker, C. I. A Retinotopic Basis for
965 the Division of High-Level Scene Processing between Lateral and Ventral Human
966 Occipitotemporal Cortex. *J. Neurosci.* **35**, 11921–11935 (2015).

967 64. Somers, D. C. & Sheremata, S. L. Attention maps in the brain. *Wiley Interdiscip. Rev. Cogn. Sci.*
968 **4**, 327–340 (2013).

969 65. Silver, M. A. & Kastner, S. Topographic maps in human frontal and parietal cortex. *Trends*
970 *Cogn. Sci.* **13**, 488–495 (2009).

971 66. Amunts, K., Mohlberg, H., Bludau, S. & Zilles, K. Julich-Brain: A 3D probabilistic atlas of the

human brain's cytoarchitecture. *Science* **369**, 988–992 (2020).

67. Sylvester, C. M. *et al.* Network-specific selectivity of functional connections in the neonatal brain. *Cereb. Cortex* **33**, 2200–2214 (2023).

68. Huang, H. *et al.* White and gray matter development in human fetal, newborn and pediatric brains. *Neuroimage* **33**, 27–38 (2006).

69. Thiebaut de Schotten, M. & Forkel, S. J. The emergent properties of the connected brain. *Science* **378**, 505–510 (2022).

70. Dubois, J. *et al.* The early development of brain white matter: a review of imaging studies in fetuses, newborns and infants. *Neuroscience* **276**, 48–71 (2014).

71. Harding-Forrester, S. & Feldman, D. E. Somatosensory maps. *Handb. Clin. Neurol.* **151**, 73–102 (2018).

72. Humphries, C., Liebenthal, E. & Binder, J. R. Tonotopic organization of human auditory cortex. *Neuroimage* **50**, 1202–1211 (2010).

73. Amunts, K. *et al.* Broca's region revisited: cytoarchitecture and intersubject variability. *J. Comp. Neurol.* **412**, 319–341 (1999).

74. Lebel, C., Treit, S. & Beaulieu, C. A review of diffusion MRI of typical white matter development from early childhood to young adulthood. *NMR Biomed.* **32**, e3778 (2019).

75. Edwards, A. D. *et al.* The Developing Human Connectome Project Neonatal Data Release. *Front. Neurosci.* **16**, 886772 (2022).

76. Howell, B. R. *et al.* The UNC/UMN Baby Connectome Project (BCP): An overview of the study design and protocol development. *Neuroimage* **185**, 891–905 (2019).

77. Walker, L. *et al.* The diffusion tensor imaging (DTI) component of the NIH MRI study of normal brain development (PedsDTI). *Neuroimage* **124**, 1125–1130 (2016).

78. Volkow, N. D., Gordon, J. A. & Freund, M. P. The Healthy Brain and Child Development Study—Shedding Light on Opioid Exposure, COVID-19, and Health Disparities. *JAMA Psychiatry* **78**, 471–472 (2021).

79. Eichert, N. *et al.* What is special about the human arcuate fasciculus? Lateralization, projections, and expansion. *Cortex* **118**, 107–115 (2019).

80. Brauer, J., Anwander, A., Perani, D. & Friederici, A. D. Dorsal and ventral pathways in language development. *Brain Lang.* **127**, 289–295 (2013).

81. Innocenti, G. M. & Frost, D. O. Effects of visual experience on the maturation of the efferent system to the corpus callosum. *Nature* **280**, 231–234 (1979).

82. LaMantia, A. S. & Rakic, P. Axon overproduction and elimination in the corpus callosum of the developing rhesus monkey. *J. Neurosci.* **10**, 2156–2175 (1990).

83. Price, D. J., Ferrer, J. M., Blakemore, C. & Kato, N. Postnatal development and plasticity of corticocortical projections from area 17 to area 18 in the cat's visual cortex. *J. Neurosci.* **14**, 2747–2762 (1994).

84. Dehay, C., Kennedy, H. & Bullier, J. Characterization of transient cortical projections from auditory, somatosensory, and motor cortices to visual areas 17, 18, and 19 in the kitten. *J. Comp. Neurol.* **272**, 68–89 (1988).

85. Innocenti, G. M. & Price, D. J. Exuberance in the development of cortical networks. *Nat. Rev. Neurosci.* **6**, 955–965 (2005).

1014 86. Webster, M. J., Bachevalier, J. & Ungerleider, L. G. Transient subcortical connections of
1015 inferior temporal areas TE and TEO in infant macaque monkeys. *J. Comp. Neurol.* **352**, 213–
1016 226 (1995).

1017 87. Kaneko, T. *et al.* Spatial organization of occipital white matter tracts in the common
1018 marmoset. *Brain Struct. Funct.* **225**, 1313–1326 (2020).

1019 88. Takemura, H., Pestilli, F. & Weiner, K. S. Comparative neuroanatomy: Integrating classic and
1020 modern methods to understand association fibers connecting dorsal and ventral visual
1021 cortex. *Neurosci. Res.* **146**, 1–12 (2019).

1022 89. Takemura, H. *et al.* Occipital White Matter Tracts in Human and Macaque. *Cereb. Cortex* **27**,
1023 3346–3359 (2017).

1024 90. Takemura, H. *et al.* A prominent vertical occipital white matter fasciculus unique to primate
1025 brains. *Curr. Biol.* (2024) doi:10.1016/j.cub.2024.06.034.

1026 91. Zatorre, R. J., Fields, R. D. & Johansen-Berg, H. Plasticity in gray and white: neuroimaging
1027 changes in brain structure during learning. *Nat. Neurosci.* **15**, 528–536 (2012).

1028 92. Blumenfeld-Katzir, T., Pasternak, O., Dagan, M. & Assaf, Y. Diffusion MRI of structural brain
1029 plasticity induced by a learning and memory task. *PLoS One* **6**, e20678 (2011).

1030 93. Fields, R. D. A new mechanism of nervous system plasticity: activity-dependent myelination.
1031 *Nat. Rev. Neurosci.* **16**, 756–767 (2015).

1032 94. Fields, R. D. Neuroscience. Change in the brain's white matter. *Science* **330**, 768–769 (2010).

1033 95. Florence, S. L., Taub, H. B. & Kaas, J. H. Large-scale sprouting of cortical connections after
1034 peripheral injury in adult macaque monkeys. *Science* **282**, 1117–1121 (1998).

1035 96. Jain, N., Florence, S. L., Qi, H. X. & Kaas, J. H. Growth of new brainstem connections in adult
1036 monkeys with massive sensory loss. *Proc. Natl. Acad. Sci. U. S. A.* **97**, 5546–5550 (2000).

1037 97. Dancause, N. *et al.* Extensive cortical rewiring after brain injury. *J. Neurosci.* **25**, 10167–
1038 10179 (2005).

1039 98. Monje, M. Myelin Plasticity and Nervous System Function. *Annu. Rev. Neurosci.* **41**, 61–76
1040 (2018).

1041 99. Bacmeister, C. M. *et al.* Motor learning drives dynamic patterns of intermittent myelination on
1042 learning-activated axons. *Nat. Neurosci.* **25**, 1300–1313 (2022).

1043 100. Murty, N. A. R. *et al.* Visual experience is not necessary for the development of face-
1044 selectivity in the lateral fusiform gyrus. *Proceedings of the National Academy of Sciences* **117**,
1045 23011–23020 (2020).

1046 101. Meisler, S. L., Kubota, E., Grotheer, M. & Gabrieli, J. A practical guide for combining functional
1047 regions of interest and white matter bundles. (2024).

1048 102. Ewbank, M. P. *et al.* Repetition Suppression in Ventral Visual Cortex Is Diminished as a
1049 Function of Increasing Autistic Traits. *Cereb. Cortex* **25**, 3381–3393 (2015).

1050 103. Dakin, S. & Frith, U. Vagaries of visual perception in autism. *Neuron* **48**, 497–507 (2005).

1051 104. Conti, E. *et al.* Network over-connectivity differentiates autism spectrum disorder from other
1052 developmental disorders in toddlers: A diffusion MRI study. *Hum. Brain Mapp.* **38**, 2333–2344
1053 (2017).

1054 105. Picci, G., Gotts, S. J. & Scherf, K. S. A theoretical rut: revisiting and critically evaluating the
1055 generalized under/over-connectivity hypothesis of autism. *Dev. Sci.* **19**, 524–549 (2016).

106. Golarai, G. *et al.* The fusiform face area is enlarged in Williams syndrome. *J. Neurosci.* **30**, 6700–6712 (2010).

107. Behrmann, M. & Avidan, G. Congenital prosopagnosia: face-blind from birth. *Trends Cogn. Sci.* **9**, 180–187 (2005).

108. Duchaine, B. C. & Nakayama, K. Developmental prosopagnosia: a window to content-specific face processing. *Curr. Opin. Neurobiol.* **16**, 166–173 (2006).

109. Yeatman, J. D. & White, A. L. Reading: The Confluence of Vision and Language. *Annu Rev Vis Sci* **7**, 487–517 (2021).

110. Ghotra, A. *et al.* A size-adaptive 32-channel array coil for awake infant neuroimaging at 3 Tesla MRI. *Magn. Reson. Med.* **86**, 1773–1785 (2021).

111. Wang, L. *et al.* iBEAT V2.0: a multisite-applicable, deep learning-based pipeline for infant cerebral cortical surface reconstruction. *Nat. Protoc.* **18**, 1488–1509 (2023).

112. Yushkevich, P. A. *et al.* User-guided 3D active contour segmentation of anatomical structures: significantly improved efficiency and reliability. *Neuroimage* **31**, 1116–1128 (2006).

113. Zöllei, L., Iglesias, J. E., Ou, Y., Grant, P. E. & Fischl, B. Infant FreeSurfer: An automated segmentation and surface extraction pipeline for T1-weighted neuroimaging data of infants 0–2 years. *Neuroimage* **218**, 116946 (2020).

114. Tournier, J.-D. *et al.* MRtrix3: A fast, flexible and open software framework for medical image processing and visualisation. *Neuroimage* **202**, 116137 (2019).

115. Pietsch, M. *et al.* A framework for multi-component analysis of diffusion MRI data over the neonatal period. *Neuroimage* **186**, 321–337 (2019).

116. Bastiani, M. *et al.* Automated processing pipeline for neonatal diffusion MRI in the developing Human Connectome Project. *Neuroimage* **185**, 750–763 (2019).

117. Veraart, J. *et al.* Denoising of diffusion MRI using random matrix theory. *Neuroimage* **142**, 394–406 (2016).

118. Andersson, J. L. R., Graham, M. S., Zsoldos, E. & Sotiropoulos, S. N. Incorporating outlier detection and replacement into a non-parametric framework for movement and distortion correction of diffusion MR images. *Neuroimage* **141**, 556–572 (2016).

119. Tustison, N. J. *et al.* N4ITK: improved N3 bias correction. *IEEE Trans. Med. Imaging* **29**, 1310–1320 (2010).

120. Dhollander, T., Raffelt, D. & Connelly, A. Unsupervised 3-tissue response function estimation from single-shell or multi-shell diffusion MR data without a co-registered T1 image. in (09 2016).

121. Smith, R. E., Tournier, J.-D., Calamante, F. & Connelly, A. Anatomically-constrained tractography: Improved diffusion MRI streamlines tractography through effective use of anatomical information. *Neuroimage* **62**, 1924–1938 (2012).

122. Grotheer, M., Kubota, E. & Grill-Spector, K. Establishing the functional relevancy of white matter connections in the visual system and beyond. *Brain Struct. Funct.* **227**, 1347–1356 (2022).

123. Warrington, S. *et al.* Concurrent mapping of brain ontogeny and phylogeny within a common space: Standardized tractography and applications. *Science Advances* **8**, eabq2022 (2022).

124. Caspers, J. *et al.* Cytoarchitectonical analysis and probabilistic mapping of two extrastriate

areas of the human posterior fusiform gyrus. *Brain Struct. Funct.* **218**, 511–526 (2013).

125. Stigliani, A., Weiner, K. S. & Grill-Spector, K. Temporal Processing Capacity in High-Level Visual Cortex Is Domain Specific. *J. Neurosci.* **35**, 12412–12424 (2015).

126. Rosenke, M., van Hoof, R., van den Hurk, J., Grill-Spector, K. & Goebel, R. A Probabilistic Functional Atlas of Human Occipito-Temporal Visual Cortex. *Cereb. Cortex* **31**, 603–619 (2020).

127. Cai, Q., Paulignan, Y., Brysbaert, M., Ibarrola, D. & Nazir, T. A. The left ventral occipito-temporal response to words depends on language lateralization but not on visual familiarity. *Cereb. Cortex* **20**, 1153–1163 (2010).

128. Petersen, S. E., Fox, P. T., Posner, M. I., Mintun, M. A. & Raichle, M. E. Positron emission tomographic studies of the cortical anatomy of single-word processing. *Nature* **331**, 585–589 (1988).

129. Benson, N. C. & Winawer, J. Bayesian analysis of retinotopic maps. *Elife* **7**, (2018).

130. Finzi, D. *et al.* Differential spatial computations in ventral and lateral face-selective regions are scaffolded by structural connections. *Nat. Commun.* **12**, 2278 (2021).